High Current Density and Low Hysteresis Effect of Planar Perovskite Solar Cells via PCBM-doping and Interfacial Improvement

He Jiang,[†,‡] *Gelei Jiang,*[†,‡] *Weiwei Xing,*[†,‡] *Weiming Xiong,*[†,‡] *Xiaoyue Zhang,*[†,‡] *Biao Wang,*[*,†,§] *Huiyan Zhang*[†,‡] *and Yue Zheng*[*,†,‡]

[†]State Key Laboratory of Optoelectronic Materials and Technologies, School of Physics and [‡]Micro and Nano Physics and Mechanics Research Laboratory, School of Physics, Sun Yat-sen University, Guangzhou 510275, China.

[§]Sino-French Institute of Nuclear Engineering and Technology, Sun Yat-sen University, Zhuhai, 519082, China.

*Correspondence and requests for materials should be addressed to Y. Z. (email: zhengy35@mail.sysu.edu.cn) or B. W. (email: wangbiao@mail.sysu.edu.cn).

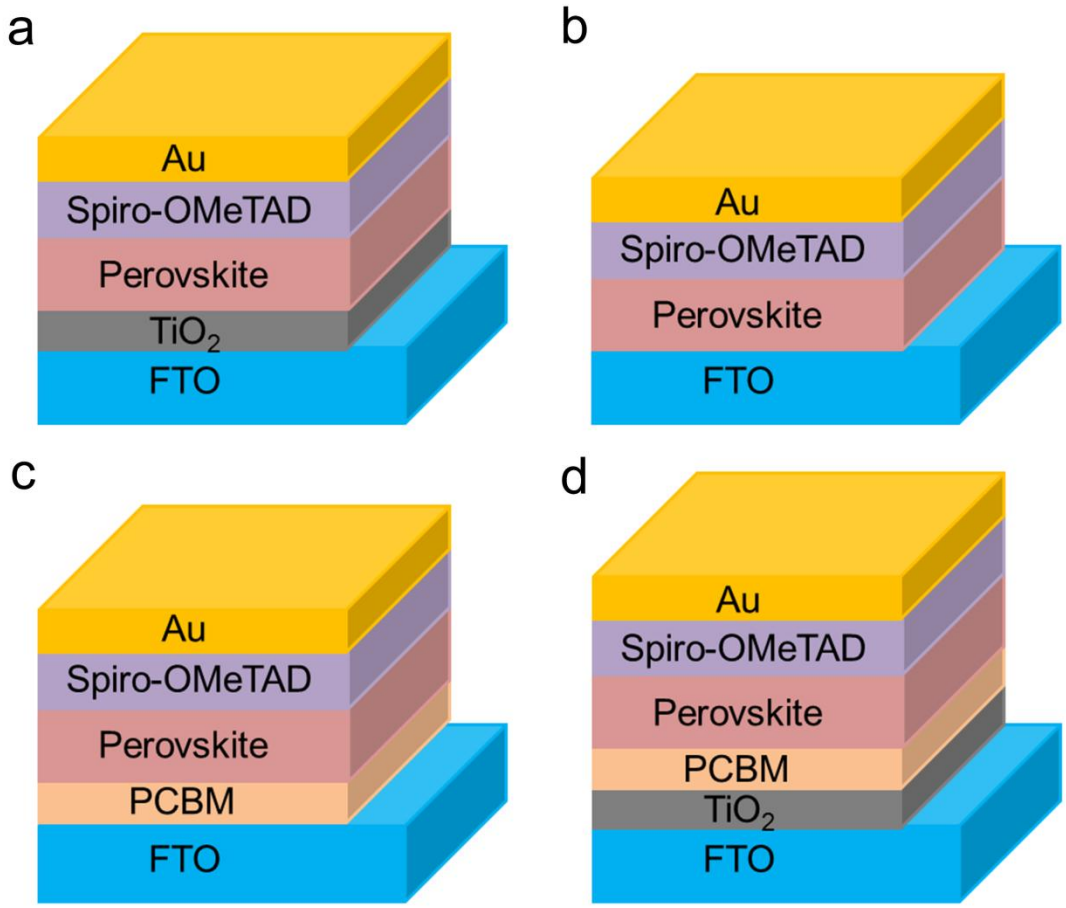

Figure S1. Schematic of planar perovskite solar cells with different ETH schemes used in this work. (a) TiO_2-based, (b) ETH-free, (c) PCBM-based and (d) TiO_2/PCBM-based schemes.

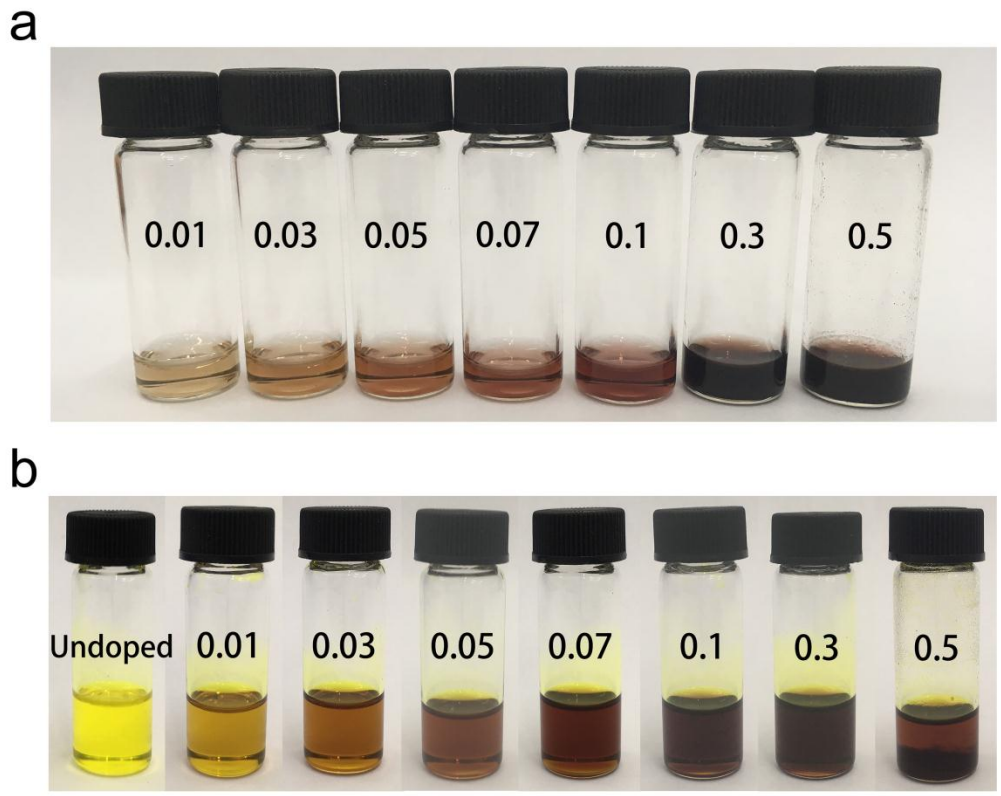

Figure S2. Photographs of PCBM solutions and perovsktie precursor solutions. (a) Study on PCBM Solubility in DMF/DMSO mixed solution. The undissolved PCBM powders are observed at 0.5 wt%. (b) Different PCBM doping concentrations of perovskite precursor solutions (0.14, 0.18, 0.22 and 0.26 wt% are not shown). One can clearly see that the obvious sediments exist in 0.5 wt% precursor solution.

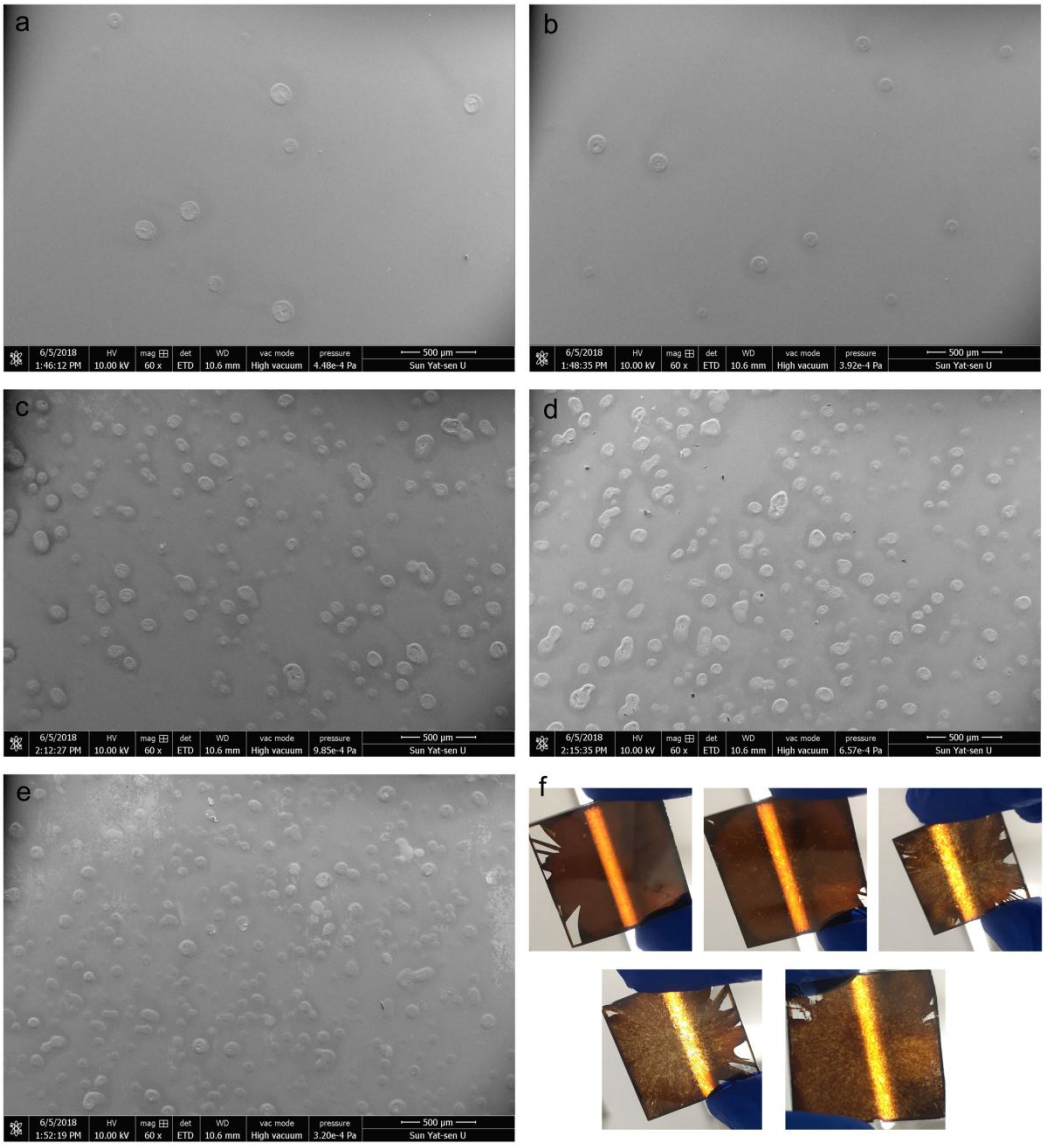

Figure S3. SEM top-view and photographs for different PCBM doping concentrations of perovskite films on FTO substrate. (a) 0.14 wt%, (b) 0.18 wt%, (c) 0.22 wt%, (d) 0.26 wt% and (e) 0.3 wt%. The scale bars is 500 μm. (f) Photographs of each PCBM-doped perovskite films. The above three are 0.14, 0.18 and 0.22 wt% samples from the left to right side, and the bottom two are 0.26 and 0.3 wt% samples from the left to right side.

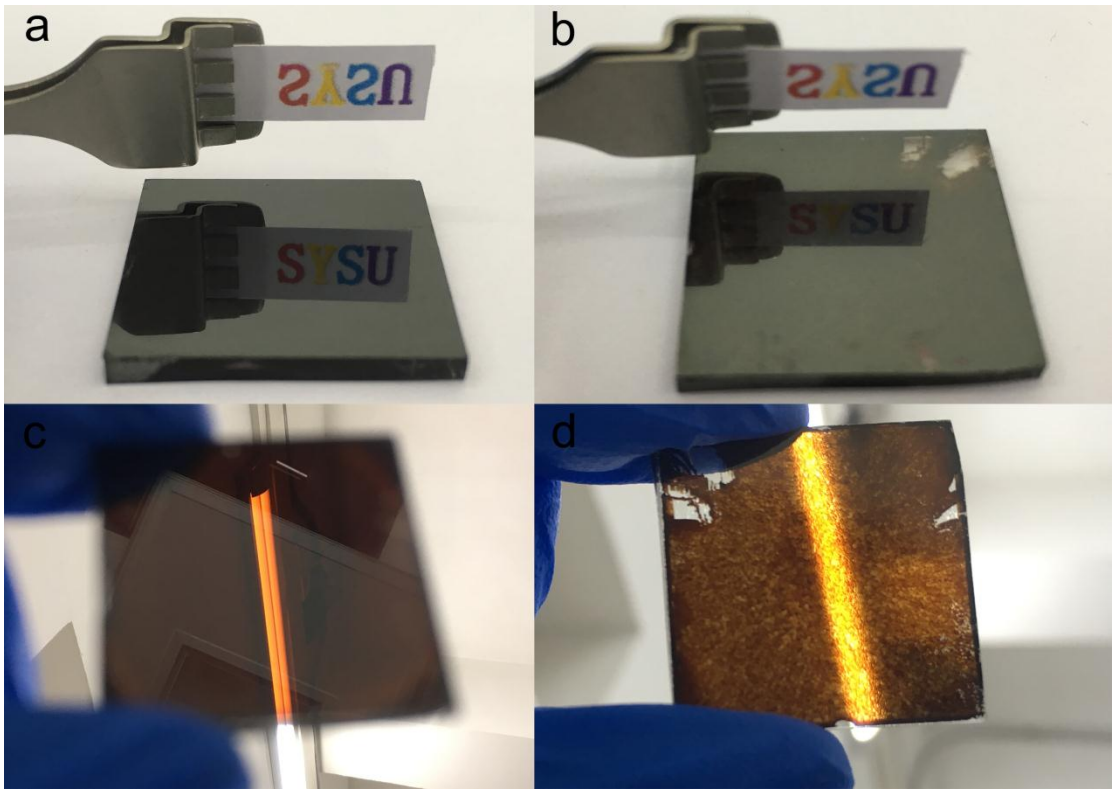

Figure S4. Photographs of perovskite films on FTO. (a,c) 0.1 wt% PCBM-doped perovskite sample. (b,d) 0.3 wt% PCBM-doped perovskite sample.

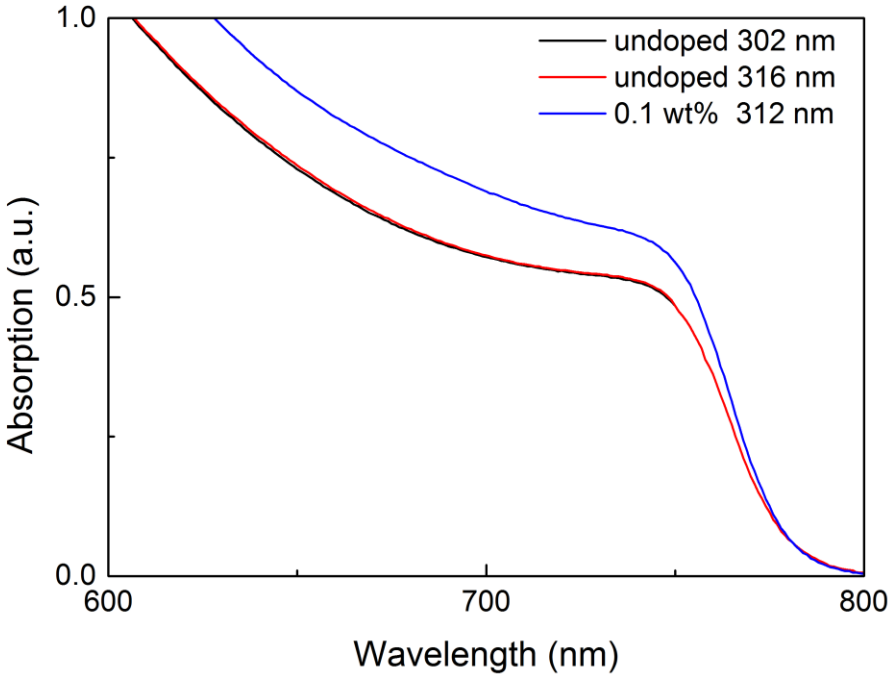

Figure S5. Absorption spectra of undoped perovskite film samples with different thickness and 0.1 wt% PCBM-doped perovskite film sample measured on FTO.

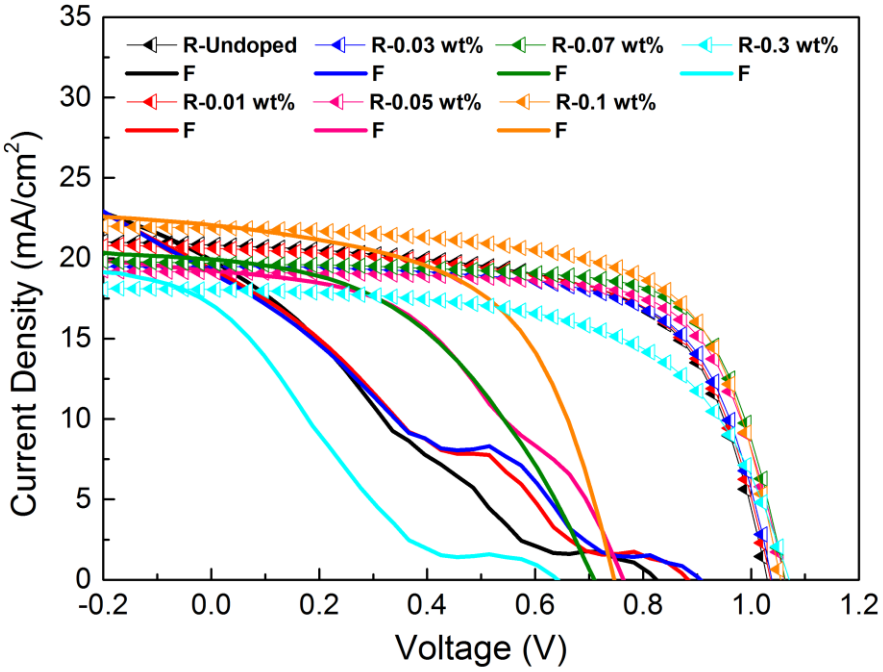

Figure S6. J-V characteristics of planar undoped and PCBM-doped perovskite solar cells without ETL measured under reverse (R) and forward (F) conditions. The slightly higher Jsc values (approximately ~1.5 mA/cm^2) in these devices can be attributed the measuring error, due to the uncorrected active area in the process of measurement.

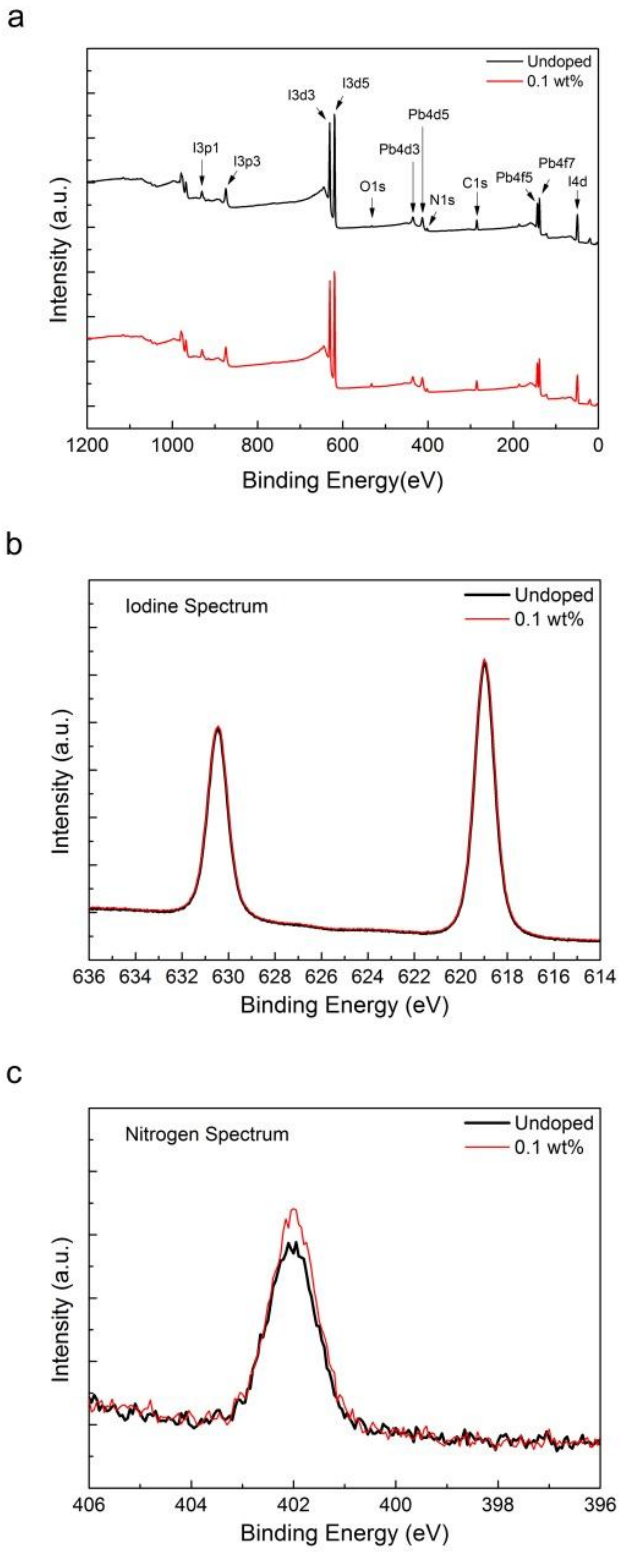

Figure S7. XPS measurement on undoped and 0.1 wt% PCBM-doped perovskite films on FTO/PCBM substrate. (a) Overview spectra, (b) iodine core level spectra and (c) nitrogen core level spectra.

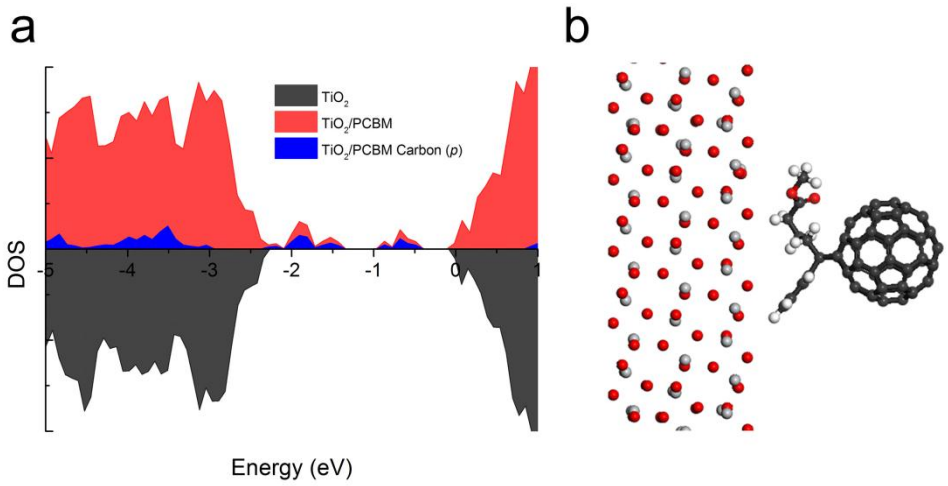

Figure S8. DFT analysis of DOS on TiO_2 (1 0 1)/PCBM adsorption structure. (a) Total DOS of TiO_2(1 0 1) surface (black area) and TiO_2 (1 0 1)/PCBM (red area) structures, and the partial DOS of Carbon *p* electrons (blue area) of TiO_2(1 0 1)/PCBM structure. (b) Schematic diagram of TiO_2 (1 0 1)/PCBM adsorption structure.

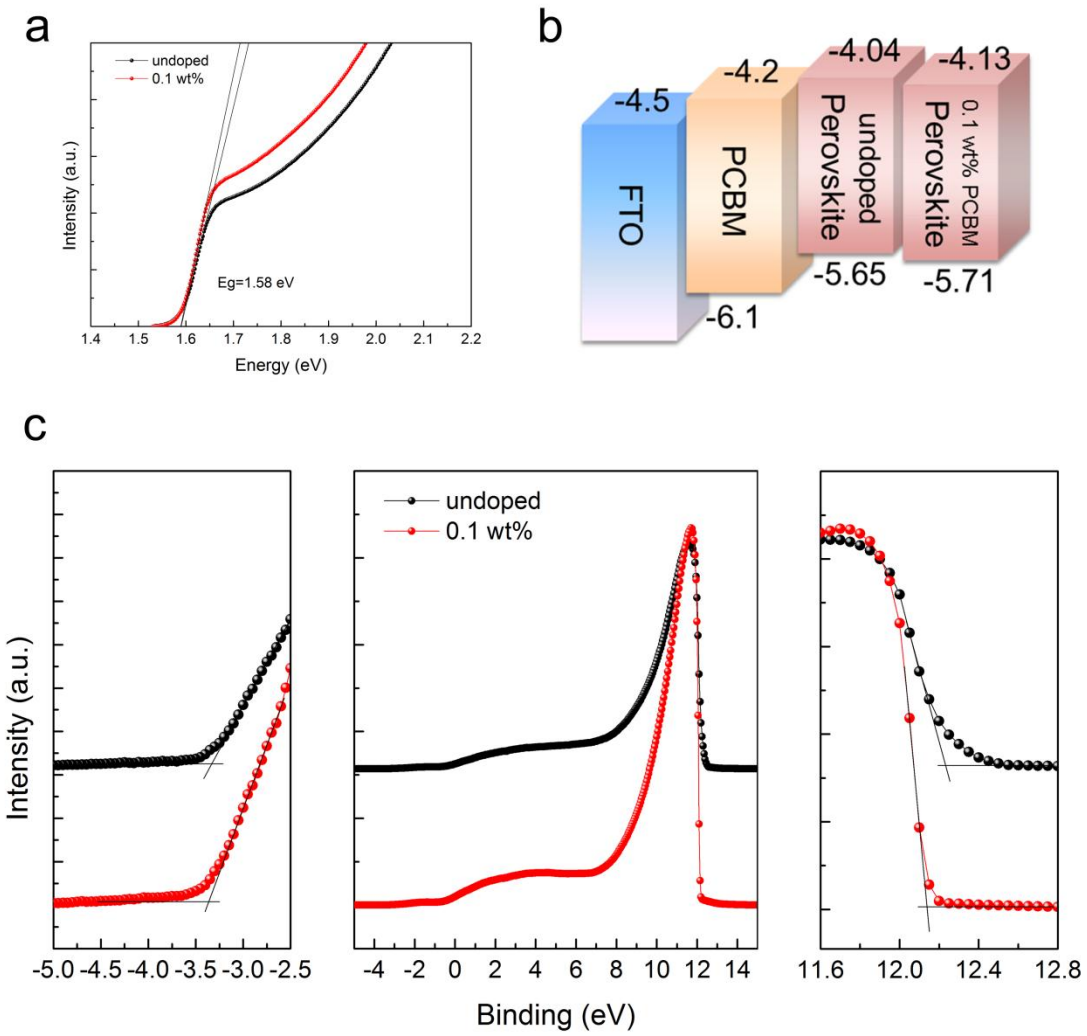

Figure S9. (a) Transformed spectra of undoped and 0.1 wt% PCBM-doped perovskites according to the absorption spectra. The band-gap (*Eg*) was determined from $h\alpha = \frac{A}{\alpha}(h\nu - E_g)^m$, where h is Planck constant, ν is photon frequency, A is a constant, m=0.5 for perovskite materials and α is absorption coefficient. (b) Schematic comparison diagram of energy level for undoped and 0.1 wt% PCBM-doped perovskites. (c) UPS spectra (with a -5 eV bias voltage) of undoped and 0.1 wt% PCBM-doped perovskite films measured on FTO/PCBM substrate, the magnifying figure of valence band edge (left), the overview spectra (midddle) and the magnifying figure of onset edge (right).

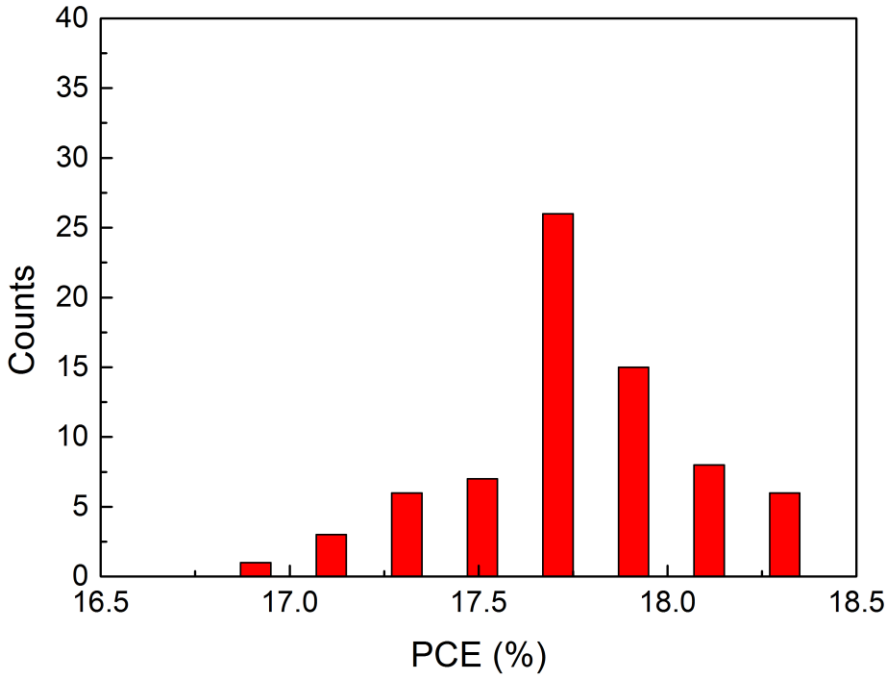

Figure S10. Histogram of the PCE values among 72 cells counted in FTO/TiO_2/PCBM/0.1 wt% PCBM-perovskite/Spiro-OMeTAD/Au device.

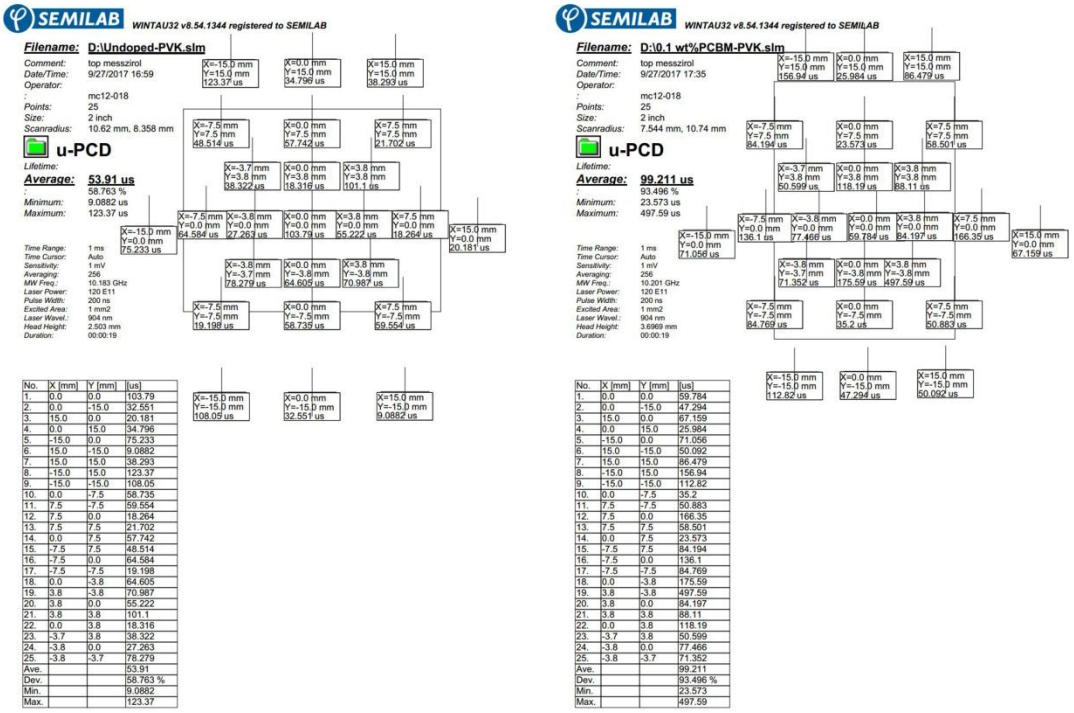

No.	X [mm]	Y [mm]	[us]
1.	0.0	0.0	103.79
2.	0.0	-15.0	32.551
3.	15.0	0.0	20.181
4.	0.0	15.0	34.796
5.	-15.0	0.0	75.233
6.	15.0	-15.0	9.0882
7.	15.0	15.0	38.293
8.	-15.0	15.0	123.37
9.	-15.0	-15.0	108.05
10.	0.0	-7.5	58.735
11.	7.5	-7.5	59.554
12.	7.5	0.0	18.264
13.	7.5	7.5	21.702
14.	0.0	7.5	57.742
15.	-7.5	7.5	48.514
16.	-7.5	0.0	64.584
17.	-7.5	-7.5	19.198
18.	0.0	-3.8	64.605
19.	3.8	-3.8	70.987
20.	3.8	0.0	55.222
21.	3.8	3.8	101.1
22.	0.0	3.8	18.316
23.	-3.7	3.8	38.322
24.	-3.8	0.0	27.263
25.	-3.8	-3.7	78.279
Ave.			53.91
Dev.			58.763 %
Min.			9.0882
Max.			123.37

No.	X [mm]	Y [mm]	[us]
1.	0.0	0.0	59.784
2.	0.0	-15.0	47.294
3.	15.0	0.0	67.159
4.	0.0	15.0	25.984
5.	-15.0	0.0	71.056
6.	15.0	-15.0	50.092
7.	15.0	15.0	86.479
8.	-15.0	15.0	156.94
9.	-15.0	-15.0	112.82
10.	0.0	-7.5	35.2
11.	7.5	-7.5	50.883
12.	7.5	0.0	166.35
13.	7.5	7.5	58.501
14.	0.0	7.5	23.573
15.	-7.5	7.5	84.194
16.	-7.5	0.0	136.1
17.	-7.5	-7.5	84.769
18.	0.0	-3.8	175.59
19.	3.8	-3.8	497.59
20.	3.8	0.0	84.197
21.	3.8	3.8	88.11
22.	0.0	3.8	118.19
23.	-3.7	3.8	50.599
24.	-3.8	0.0	77.466
25.	-3.8	-3.7	71.352
Ave.			99.211
Dev.			93.496 %
Min.			23.573
Max.			497.59

Figure S11. Testfile of minority carrier lifetimes for undopd (left) and 0.1 wt% PCBM-doped perovskites (right).

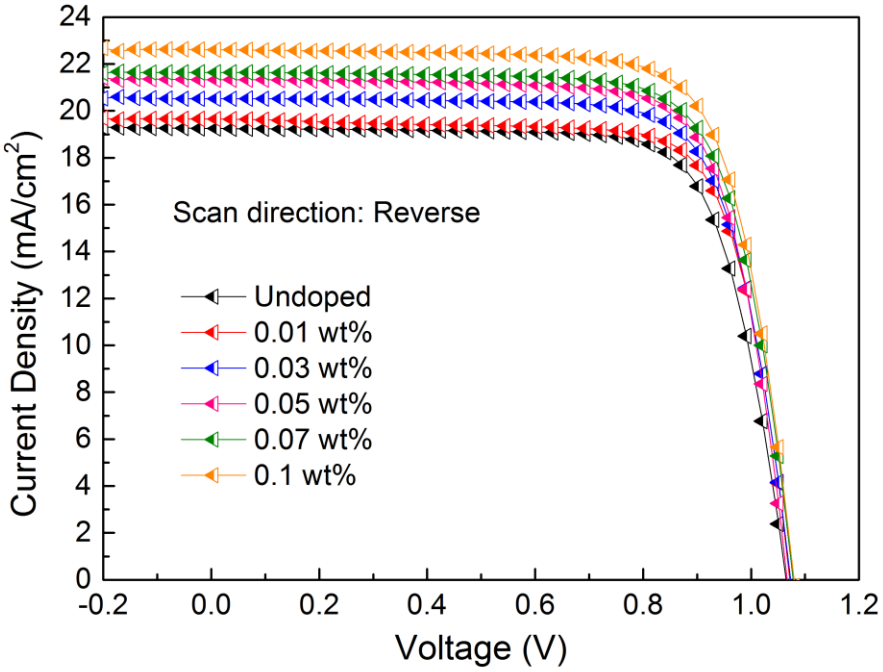

Figure S12. J-V characteristics of planar undoped and PCBM-doped perovskite solar cells with TiO_2/PCBM-based ETL measured under reverse condition.

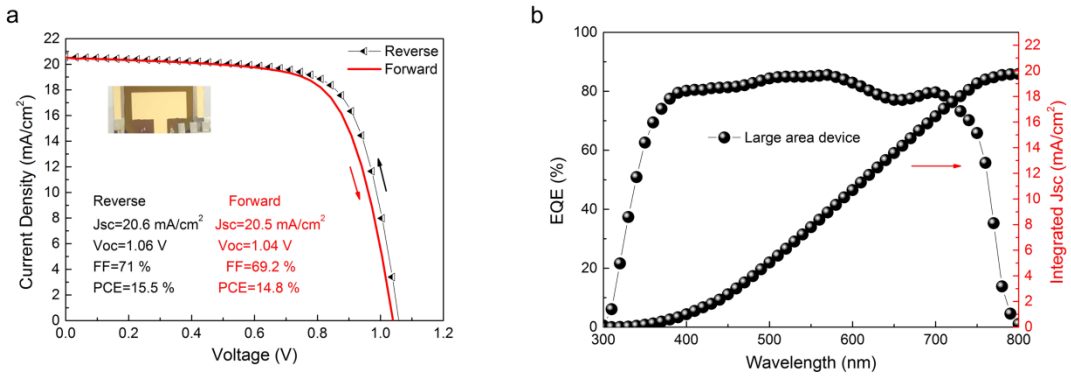

Figure S13. The optimal performance of large area device in this work. (a) J-V characteristics of lareg-area (1.05 cm^2) TiO_2/PCBM-based 0.1 wt% PCBM-doped perovskite solar cell. A quadrate mask with 0.84 cm^2 was used to correct the active area in the process of measurement. The inset is photograph of device. (b) External quantum efficiency (EQE) spectra and integrated Jsc for the corresponding device.

Table S1. The thickness of perovskite films with different PCBM doping concentrations measured on FTO.

PCBM Concentrations (wt%)	**Thickness (nm)**					**Average (nm)**
0	305	300	303	299	301	**302**
0.01	302	307	307	300	306	**304**
0.03	298	300	298	301	300	**299**
0.05	304	305	305	303	306	**305**
0.07	303	301	305	303	308	**304**
0.1	312	314	310	314	311	**312**

Table S2. Summary of TiO_2/PCBM-based planar perovskite solar device parameters measured under reverse condition.

PCBM Concentrations (wt%)	Jsc (mA/cm^2)	Voc (V)	FF (%)	PCE (%)
0	19.3	1.07	75.3	15.6
0.01	19.6	1.07	75.8	15.9
0.03	20.5	1.07	75.4	16.5
0.05	21.3	1.07	75.4	17.2
0.07	21.6	1.08	74.9	17.5
0.1	22.6	1.08	75.1	18.3

Calculation Description

First-principle calculation within density functional theory (DFT) was used to investigate all structures by employing the Vienna Ab initio Simulation Package (VASP) in this work.[1] The structural optimization process was performed by using generalized gradient approximation (GGA)[2] with projector augmented wave (PAW)[3] pseudopotentials. The plane wave energy cutoff of 310 eV was used for all modeling surface and adsorption structures. The converged $1 \times 1 \times 1$ and $2 \times 2 \times 2$ Monkhorst–Pack[4] grid for k-point samplings were used for structural relaxation and density of state (DOS), respectively. All structures were configured 80 Å thickness of vacuum layer along c-axis. The structure of PCBM molecule adsorbed on TiO_2 surface was modeled by using anatase TiO_2 (1 0 1) surface, which is the mainly exposed surface in nature and applied surface in the field of solar cell devices.[5, 6] For the perovskite/PCBM adsorption structure, the PbI_2-terminated $CH_3NH_3PbI_3$ (0 0 1) surface, which the relatively stable surface possessing a small surface energy[7] with the Pb-I antisite defects (the most anticipated defect[8]) was used, meanwhile, establishing one or twain adsorbed PCBM molecules on surface to represent the change of doping concentrations. For the adsorption orientation of one PCBM molecule, O-facing scheme was used in this work that referred the previous report.[9] Van der Walls interactions were included Semi-empirically by using the dispersion-corrected density functional theory (DFT-D).[10] All atoms were relaxed until the Hellmann–Feynman force on each atom was less than 10 meV/Å.

References

(1) Kresse, G.; Furthmuller, J. Efficient Iterative Schemes for Ab Initio Total-energy Calculations Using A Plane-wave Basis Set. *Phys. Rev. B* **1996,** *54* (16), 11169-11186.

(2) Perdew, J. P.; Chevary, J. A.; Vosko, S. H.; Jackson, K. A.; Pederson, M. R.; Singh, D. J.; Fiolhais, C. Atoms, Molecules, Solids, and Surfaces: Applications of The Generalized Gradient Approximation for Exchange and Correlation. *Phys. Rev. B* **1992,** *46* (11), 6671-6687.

(3) Blochl, P. E. Projector Augmented-wave Method. *Phys. Rev. B* **1994,** *50* (24), 17953-17979.

(4) Monkhorst, H. J. Special Points for Brillouin-zone Integrations. *Phys. Rev. B* **1976,** *16* (4), 1748-1749.

(5) Grätzel, M. Dye-sensitized Solar Cells. *J. Photoch. Photobio. C* **2003,** *4* (2), 145-153.

(6) Lazzeri, M.; Vittadini, A.; Selloni, A. Structure and Energetics of Stoichiometric TiO_2 Anatase Surfaces. *Phys. Rev. B* **2001,** *65* (11), 155409.

(7) Haruyama, J.; Sodeyama, K.; Han, L.; Tateyama, Y. Termination Dependence of Tetragonal $CH_3NH_3PbI_3$ Surfaces for Perovskite Solar Cells. *J. Phys. Chem. Lett.* **2014,** *5* (16), 2903-2909.

(8) Buin, A.; Pietsch, P.; Xu, J.; Voznyy, O.; Ip, A. H.; Comin, R.; Sargent, E. H. Materials Processing Routes to Trap-free Halide Perovskites. *Nano. Lett*. **2014,** *14* (11), 6281-6286.

(9) Xu, J.; Buin, A.; Ip, A. H.; Li, W.; Voznyy, O.; Comin, R.; Yuan, M.; Jeon, S.; Ning, Z.; McDowell, J. J.; Kanjanaboos, P.; Sun, J. P.; Lan, X.; Quan, L. N.; Kim, D. H.; Hill, I. G.; Maksymovych, P.; Sargent, E. H. Perovskite-fullerene Hybrid Materials Suppress Hysteresis in Planar Diodes. *Nat. Commun.* **2015**, *6*, 7081.

(10) Barone, V.; Casarin, M.; Forrer, D.; Pavone, M.; Sambi, M.; Vittadini, A. Role and Effective Treatment of Dispersive Forces in Materials: Polyethylene and Graphite Crystals as Test Cases. *J. Comput. Chem.* **2009,** *30* (6), 934-939.